ELECTRON EMISSION PROPERTIES OF INSULATOR MATERIALS PERTINENT TO THE INTERNATIONAL SPACE STATION

C.D. Thomson
Physics Department, Utah State University
Logan, UT, USA 84322-4415
Phone: 435.797.2936
Fax: 436.797.2492
E-mail: JR.Dennison@usu.edu

V. Zavyalov
J.R. Dennison
Jodie Corbridge
Physics Department, Utah State University

Abstract

We present the results of our measurements of the electron emission properties of selected insulating and conducting materials used on the International Space Station (ISS). Utah State University (USU) has performed measurements of the electron-, ion-, and photon-induced electron emission properties of conductors for a few years, and has recently extended our capabilities to measure electron yields of insulators, allowing us to significantly expand current spacecraft material charging databases. These ISS materials data are used here to illustrate our various insulator measurement techniques that include:

i) Studies of electron-induced secondary and backscattered electron yield curves using pulsed, low current electron beams to minimize deleterious affects of insulator charging.

ii) Comparison of several methods used to determine the insulator 1st and 2nd crossover energies. These incident electron energies induce unity total yield at the transition between yields greater than and less than one with either negative or positive charging, respectively. The crossover energies are very important in determining both the polarity and magnitude of spacecraft surface potentials.

iii) Evolution of electron emission energy spectra as a function of insulator charging used to determine the surface potential of insulators.

iv) Surface potential evolution as a function of pulsed-electron fluence to determine how quickly insulators charge, and how this can affect subsequent electron yields.

v) Critical incident electron energies resulting in electrical breakdown of insulator materials and the effect of breakdown on subsequent emission, charging and conduction.

vi) Charge-neutralization techniques such as low-energy electron flooding and UV light irradiation to dissipate both positive and negative surface potentials during yield measurements.

Specific ISS materials being tested at USU include chromic and sulfuric anodized aluminum, RTV-silicone solar array adhesives, solar cell cover glasses, Kapton™, and gold. Further details of the USU testing facilities, the instrumentation used for insulator measurements, and the NASA/SEE Charge Collector materials database are provided in other Spacecraft Charging Conference presentations (Dennison, 2003b). The work presented was supported in part by the NASA Space Environments and Effects (SEE) Program, the Boeing Corporation, and a NASA Graduate Fellowship. Samples were supplied by Boeing, the Environmental Effects Group at Marshall Space Flight Center, and Sheldahl, Inc.

Introduction

The electron emission properties of materials have been studied for over fifty years and are relevant to many technical applications including the continued development of electron multiplier detectors (Shih, 1997), scanning electron microscopy (Reimer, 1985; Seiler, 1983), electron probe microanalysis, Auger electron spectroscopy (Belhaj, 2000), plasma fusion devices, high-current arcing, and flat panel displays (Auday, 2000). The specific motivation for our work at Utah StateUniversity (USU) comes from NASA's concern for the charging of spacecraft materials in the space environment (Dennison, 2003d; 2002). The extent and configurations of spacecraft charge buildup depends on the spacecraft orbit, orientation, ion, electron and photon flux, and on electrical material properties such as resistivity and dielectric constant, and electron emission rates. At USU, we have expanded the material electron emission database used by NASA's current model for spacecraft charging, NASCAP 2K, to include numerous uncharacterized materials that are used in spacecraft construction. Our ground-based experiments provide us with an understanding of fundamental particle and material interactions that can occur in space (Dennison, 2003b; 2002).

The focus of recent research has been the development of instrumentation and techniques for measuring the electron-induced electron emission properties of thick and thin-film insulating materials. These efforts have led to the development of novel electronics and methodologies for making very short-duration, low-signal measurements as well as various charge-neutralization techniques (Zavyalov, 2003). To demonstrate these capabilities, we present the results of measurements made for selected insulating and conducting materials used on the International Space Station (ISS). These data demonstrate the electron-yield charging characteristics of conducting and insulating materials, as well as various techniques used to measure electron emission parameters that are used in spacecraft charging models.

Electron Emissions From Insulators and Conductors

When charged particles impinge on a solid they can impart energy, exciting electrons within the material. If this energy is sufficient to overcome surface energy barriers (*e.g*. work function or electron affinity) electrons can escape from the material, leading to material charging. The emitted electrons can be divided into two categories: i) Secondary electrons (SE); typically lower energy electrons (<50 eV by convention) that originate within the material, produced by numerous inelastic scattering events of the incident electrons; ii) Backscattered electrons (BSE); typically higher energy electrons (>50 eV by convention) that originate from the incident electron source, but scatter either elastically or inelastically before leaving the target material

(Reimer, 1985; Seiler, 1983). SE and BSE yields are defined as the ratios of the sample emitted electrons to the total incoming electrons. Such measurements on conductors are straightforward since a constant electron current source can be used and DC currents from the sample can be captured and quantified using a retarding-grid detector assembly (with a zero or -50 V suppression used to discriminate between SE's and BSE's) and picoammeters. Additionally, by grounding the conductor, any charge that leaves or is absorbed into the material can be immediately neutralized to ground.

Electron yield measurements on dielectrics are more difficult to make, since any charge that is deposited in the material cannot easily be dissipated. The surface and bulk potentials that develop can subsequently affect electron emissions by influencing incident electron energies, or by creating electric fields that affect the escaping SE's. Without the implementation of neutralization techniques, an irradiated insulator will eventually charge to a steady state current equilibrium such that the net current to the sample is zero or the total electron yield is equal to one (Reimer, 1985; Seiler, 1983).

The polarity of insulator charging is dependent on incident electron energies. Positive (negative) charge will build up when the total number of electrons leaving the insulator sample is greater than (less than) the total number of incoming electrons. If the energy of incident electrons is below the insulator first crossover energy, E_1, (<100 V for most good insulators) negative charging results, since few SE's are excited by absorbed electrons. Likewise, if the incoming electron energies are above the second crossover energy, E_2 (>1 keV for most insulators) negative charging will again result since incident electrons penetrate deep into the material (up to several microns), exciting SE's (escape length tens of nanometers) that are too deep to escape from the material. However, if the incident electrons have energies between E_1 and E_2, more electrons will be emitted from the insulator than are incident, and net positive charging will occur. SE yield curves are commonly parameterized by the energy, E_{max}, that gives a maximum SE yield δ_{max} (or total yield, σ_{max}) as well as by the first and second crossover energies, E_1 and E_2. Furthermore, the magnitude of insulator charging can depend on a number of other parameters that include the BSE and SE yield properties, incident beam angle (Davies, 1999; Yong, 1998), substance purity, crystalline structure (Whetten and Laponsky, 1959), temperature (Johnson, 1953; Johnson, 1948; Mueller, 1945), insulator thickness (Yu, 2001; Goto, 1968; Ishikaw, 1967), surface cleanliness (Davies, 1997; Whetten, 1964; Whetten, 1959; 1957), sample potential (Yi, 2001), surface topography (Yong, 1998), and previous electron irradiation exposure leading to increased defect density and imbedded charge (Shih, 1997; Vigouroux, 1985). Numerous conductor electron spectra, yield curves, and yield parameters have been measured at USU and are available on the NASA SEE Charge Collector Knowledge Base (Dennison, 2002).

DC and Pulsed-Yield Measurement Setup and Sample Preparation

The general electron yield measurement procedure is briefly described here, but is covered more thoroughly in other SCC conference proceedings (Zavyalov, 2003, Dennison, 2003b). All measurements of thin-film conductor foils and insulator films were performed in the USU UHV test chamber at pressures ranging from 10^{-10} to 10^{-8} Torr, depending on the sample data set. Two electron guns were available for making yield measurements: a low-energy gun (STAIB EK-5-S,

energy range 50 eV to 5 keV), and a high-energy gun (Kimball ERG-21, energy ranging from 4 keV to 30 keV). Both guns provided beam currents ranging from 10-100 nA, with beam spot diameters ranging from 0.1 to 2 mm (depending on the energy), and pulsing capabilities from 1 μs to continuous emission. Emitted electrons were captured using a fully enclosing hemispherical grid detection system with a suppression grid used to discriminate between BSE's (energies >50 eV) and SE's (energies <50 eV) and to make energy-resolved measurements. For conducting samples, electron guns were operated in continuous emission mode, and dc-currents were measured with standard ammeters sensitive to several tens of picoamperes. For pulsed measurements on insulators, the electron guns delivered 5 μs, 20-60 nA incident pulses. A low-energy electron flood gun (energies <1 eV) was used to neutralize positive surface charging between pulses (Zavyalov, 2003; Dennison, 2003b; Krainsky, 1981).

Four specific materials used on the ISS—gold foil, a chromic acid anodized aluminum disk, and RTV thin films—were studied. The gold foil and Al alloy disk were glued to copper sample mounts using UHV compatible conductive silver adhesive paint. Both samples were cleaned using acetone and methanol immediately before introduction into the vacuum. Additionally, the gold sample was sputtered *in situ* with argon to remove adsorbed contamination monolayers, and sample cleanliness was confirmed using Auger spectroscopy. The thin-film RTV coatings on copper substrates were prepared by McDonald Douglass Corporation and included two DC 93-500 silicone space-grade encapsulant films and two NuSil CV-1147 controlled volatility RTV silicone films (Dennison, 2003c). The coatings were sprayed onto 10 mm dia. copper substrates (one side only), and were vacuum baked at 65 °C for 1 hr at ~10^{-3} Torr. The bake out procedure was designed in part to mimic conditions that the materials would experience in the space environment and also reduced possible outgassing of volatile components in the USU vacuum chamber during electron emission measurements (Dennison, 2003c). No cleaning methods at USU were used for the DC 93-500 or NuSil CV-1147 samples before introduction to vacuum. Further descriptions of each of the samples are given in Dennison (2003c) and in the sections that follow.

Finally, similar measurements are in progress or are planned for the near future for other ISS materials, including sulfuric acid anodized Al (NASA MSFC, 2002-2003), Kapton™, solar cells and cover glasses (Dennison, 2003b).

Gold Sample: Conductor Yields and Surface Potential-Induced Spectral Shifts

The gold sample was a high-purity polycrystalline gold foil (10 mm dia., 0.1 mm thick). Au is used as a standard conductor for validation and calibration tests for electron-yield measurements (Zavyalov, 2003). Au coatings are also used on the soon-to-be-employed ISS Floating Potential Measurement Unit (FPMU) plasma charging monitor (Swenson, 2003) and on other spacecraft surfaces. SE and BSE yields of Au were taken over energies ranging from 100 eV to 10 keV using the dc-measurement setup described above (Zavyalov, 2003; Dennison, 2003b). Shown in Fig. 1 is the SE energy distribution for gold while being irradiated with a continuous 80 eV electron source. As can be seen from the spectrum, the SE energy distribution peaks at 2.3±0.5 eV, and ~70% electrons are emitted with energies ranging from 0-20 eV. Similar emission spectrum attributes are characteristic of both insulator and conductor materials. Shown in Fig. 2 are the total, SE and BSE yields as a function of incident beam energy. As can

be seen in the figure, the SE and total yields increase with increasing incident electron energy up to 600 eV, but then fall off as the beam penetration depth exceeds the mean SE escape depth (<10 nm).

Measuring shifts in the SE spectral emission peak provides a method for determining the sample surface potential of any material (particularly of charged insulator materials) while under continuous electron bombardment. Sample potentials can have considerable affects on SE escape kinetic energies. Typically, a material with 0 V surface potential displays a SE emission peak near 2 eV (Fig. 1). However, if the sample potential is negative, SE's will be accelerated away from the sample surface. The increased energy of escaping SE's can be observed in the spectra as a shift of the SE emission peak to higher energies. Alternatively, a few-volt positive sample potential will pull the majority of SE's back to the surface. A positive potential from the retarding grid can be used to extract the SE's from the sample, producing a shift of the SE emission peak to the left in the spectra (Girard, 1992; O. Jbara, 2001; Y. Mizuhara, 2002).

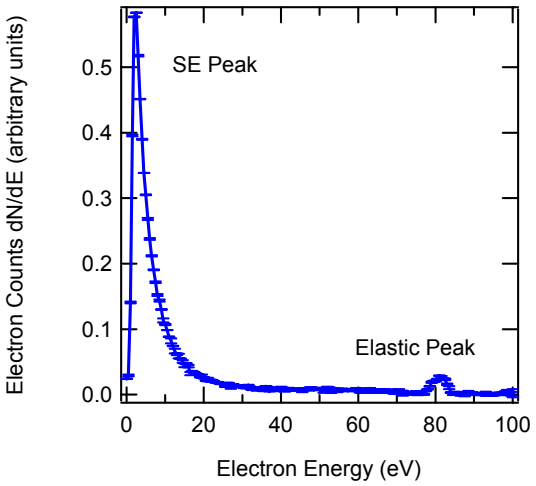

Figure 1. Electron energy spectrum for Au, induced from a 80 eV electron beam. SE peak at 2.3±0.5 eV.

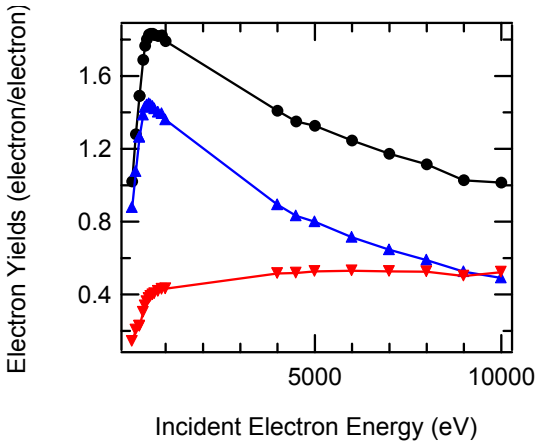

Figure 2. Total (●), SE (▲), and BSE (▼) electron yields for Au as a function of incident electron beam energy. Total yield parameters are σmax=1.8±0.1 at Emax=600±50 eV.

This SE spectral method for determining negative sample potentials was demonstrated on gold, and was used later on insulating samples to determine surface potentials induced by a continuous electron beam. Shown in Fig. 3 are four SE emission spectra taken with a 1 keV incident beam while biasing the sample negatively to 2 V, 5 V, 10 V, and 15 V. Due to the repulsion of emitted SE's from the negatively biased sample, the SE peak is right-shifted to values corresponding to the applied sample potential (see Fig. 3). A "false" SE emission peak is observed at 1.8±0.5 eV in all the spectra caused by electron scattering from the grounded inner detector grid, positioned between the sample and the retarding grid. This false SE peak did not vary with sample type or bias, and was taken as a ground-reference potential for shifted sample SE peaks. Also, the height of the grid SE peak, with respect to the shifted sample SE peaks, provided a relative measure of the number of SE's emitted from the material. Incidentally, since this inner grid remained grounded throughout the experiments, and screened out retarding-grid accelerating potentials, positive sample potentials were not measured in this way.

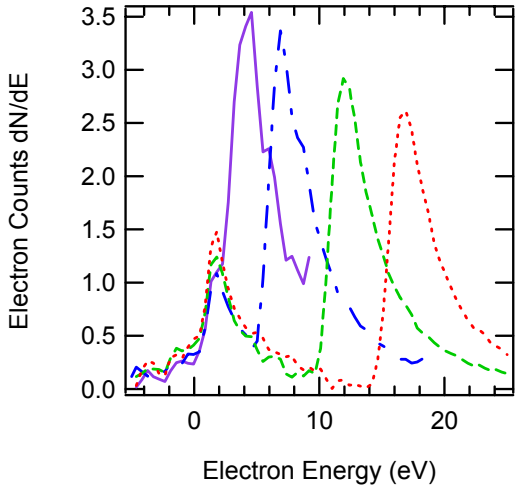

Figure 3. SE spectra on negatively biased gold for -2 V (solid), -5 V (dash-dot), -10 V (short dash), and -15 V (dot). Measured with respect to the grounded grid peak (1.8 eV), the SE peak positions correspond to the applied potentials, accurate to ± 1eV.

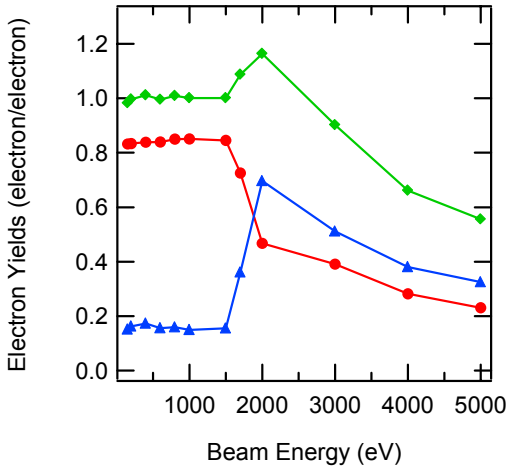

Figure 4. DC-total (♦), SE (●), and BSE (▲) yields for Al2219. The sample remained charged until 1500 eV, where dielectric breakdown occurred.

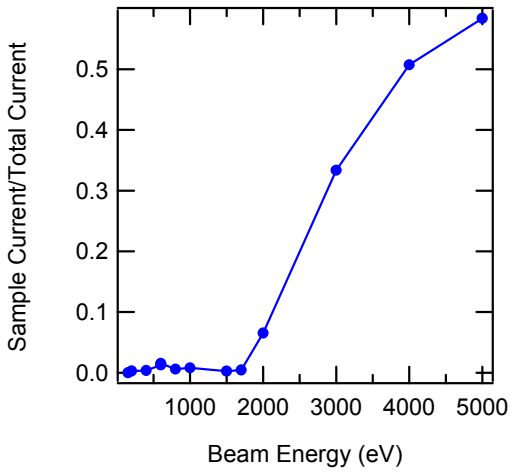

Figure 5. Monitoring Al2219 sample current confirmed dielectric breakdown at 1600 eV, where the sample began to conduct DC current.

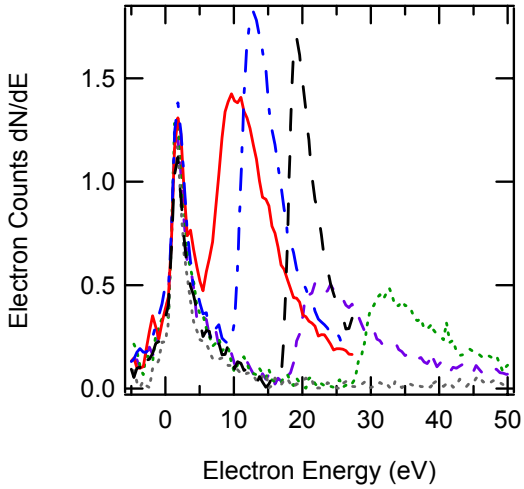

Figure 6. SE DC spectra of Al2219 showed increasingly negative surface potentials at beam energies of 200 eV (9±1 V) (solid), 500 eV (11±1 V) (dash-dot), 1000 eV (17±1 V) (long dash), 1250 eV (21±2 V) (short dash), 1300 eV (32±2 V) (dot). Decline of SE peak magnitude at 1250 eV indicated dielectric breakdown once more at a surface potential of 21±2 V.

Al2219 Insulator Yields, Emission Spectra, Electrical Breakdown, and Trapped Charge

A chromic acid anodized Al2219 alloy is used throughout the ISS body as a structural material and for micrometeriod and orbital debris shielding. The Al2219 alloy sample (2 mm thick, 10 mm diameter with a 1.3 μm chromic acid anodized surface coating on each side) was taken from a witness sample plate that was created at the same time as the large plates used on the ISS (NASA, 2002-2003). Specific aims in studying this sample were to compare the results of the dc- and pulsed-yield measurements for insulator to determine the effectiveness of the pulsed-yield setup. Additionally, evolving sample potentials under both continuous- and pulsed-incident electron beams were studied. Finally, discharging techniques including electron flooding, UV, and visible light irradiation were explored.

DC-yields were taken first using a continuous electron source at ~20 nA beam current. As shown in Fig. 4, for energies ranging from 100 eV to 1500 eV, the insulator quickly charged such that a steady-state current equilibrium was established where the total yield reached unity, and no net current flowed to or from the sample. However, after 1600 eV, a transition in the yield values occurred. As shown in Fig. 5, the sample current suddenly increased, indicating dielectric breakdown of the anodized coating. For this measurement, the exact value of the surface potential at electrical breakdown was not measured, but from the known thickness and dielectric strength for Al_2O_3 (see Table 1) was estimated to be ~35 V. Previous measurements on this material have demonstrated a breakdown potential ranging from 60-80 V (Schneider, 2003).

After letting the sample sit for a day, the breakdown surface potential was once again explored using a continuous incident electron beam and measuring the SE spectra. The incident beam energy was increased for each successive spectral measurement (starting from 200 eV up to 1300 eV) until signs of breakdown occurred. As shown in Fig. 6, (and as demonstrated with the gold sample), right-shifting of the SE emission peak was used to determine the magnitude of the sample potential.

Table 1. Insulator sample characteristics. RTV sample thicknesses, resistivities, dielectric constrants, dielectric strengths are from Dennison (2003c), Alred (2001), Dow Corning (1998), and NuSil (1998, 2001). Anodized A1 thickness is from Schneider (2003), resistivity from Goodfellow (2003), dielectric sonstrant from Carruth (2001), and dielectric strength from alumina data CRC (2001). Breakdown potentials were calculated from dielectric strengths and thicknesses. The estimate alumina data CRC (2001). Breakdown potentials were calculated from dielectric strengths and thicknesses. The estimate for E_2 for anodized A1 was obtained from the best fitting model (Variable n) to the yield curve data. Estimates for E_2 for RTV samples were obtained using total yield (Variable n model), spectral, and mirror-method techniques. Uncertainties in the mirror method data were obtained from decays in the surface potential over a measurement period of 1-3 min.

Samp.	Material	Thick. (μm)	Resist. (Ω·cm)	Rel. Diel. Const.	Diel. Strength (MV/m)	Brkdwn. Pot. (V)	Tot. Yld E_2 (eV)	DC-Spectral E_2 (eV)	Mirror Meth. E_2 (eV)
Al2219	Chromic Acid Anod. Al	1.3±0.5	$>10^{14}$	5.0-9.3	13	35	1400±100	No data	No data
RTV 1	CV-1147	34±3	10^{15}	2.6	22	743	1470±40	1225±25	1200±200
RTV 2	CV-1147	30±3	10^{15}	2.6	22	644	No data	No data	1100±200
RTV 5	DC93-500	49±3	10^{15}	2.6	19	917	No data	No data	1400±400
RTV 6	DC93-500	26±3	10^{15}	2.6	19	499	1050±30	1275±25	Data not conclusive

From the data, it was observed that the sample potential remained negative at energies between E_1 and E_2, and increased in magnitude with increasing incident energy. It must be noted that a negative potential was not expected between the crossover energies since the total electron yield for nearly all materials is greater than unity in this energy regime (and positive surface charging should occur). However, previous experimental studies on Al_20_3 have shown that the measured

polarity of charging does not always correspond to that predicted by the electron yield parameters (Cazaux, 1999; Melchinger, 1995). A possible explanation for such behavior for our specific sample is that the previous electron irradiation produced residual trapped charge (embedded in the bulk) that provided a cumulative negative sample potential regardless of any positive SE surface charging taking place at beam energies between the crossovers. Data presented in the next two paragraphs support this hypothesis.

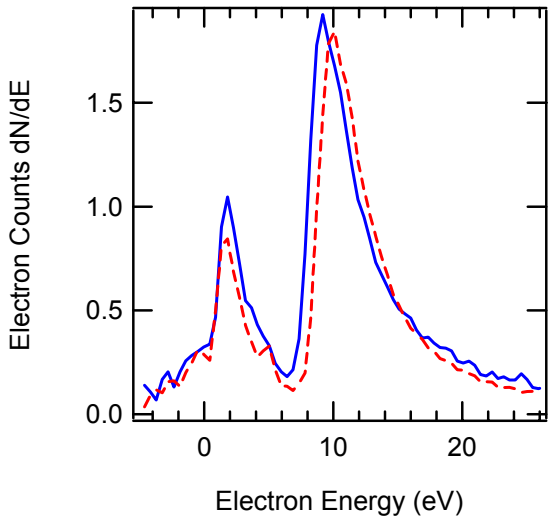

Figure 7. DC-Spectra taken at 500 eV (solid) and 1000 eV (dash) after 5 keV irradiation on Al2219 showed "locked" negative surface potential of 7-9 V resulting from imbedded electron charge.

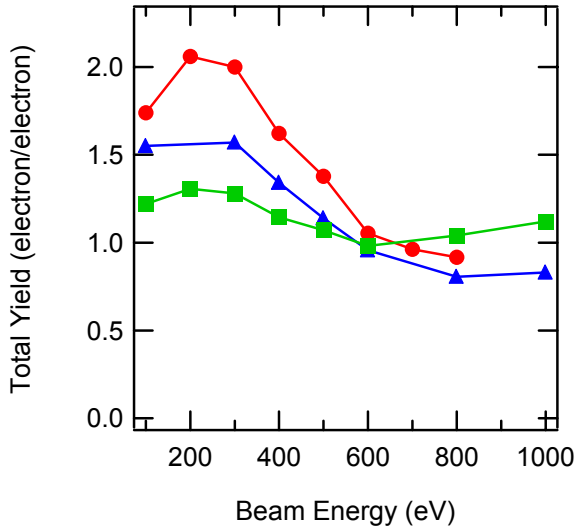

Figure 8. Three consecutive yield curves for Al2219. Each data point consists of one pulse (~106 electrons/pulse). No neutralization methods were used. The first (●), second (▲), and third (■) yield curves quickly flatten towards unity as the sample charged.

As shown in Fig. 6, as the beam energy was increased to 1250 eV and 1300 eV the surface potential reached -21±2 V and -31±2 V, respectively and the SE peaks for these energies showed a significant decrease in relative amplitudes, indicative of the electrical breakdown. From the SE spectral data, the breakdown surface potential occurred near -21 V (at beam energy 1250 eV). This value was slightly lower than the calculated estimates of -35 V, and 3-4 times smaller than previously measured values (Schneider, 2003). The value may be slightly lower since the sample had previously been irradiated and broken down on the day before at 1600 eV (see Figs. 4 and 5).

Once breakdown had occurred, the sample was irradiated for 15 min. at 5 keV beam energy to determine if subsequent SE spectra would be affected. Subsequently, the incident beam was once again lowered to 500 and 1000 eV, and SE spectra were measured. As seen in the spectra of Fig. 7, the sample potentials (both at 500 eV and 1000 eV) no longer showed dependence on incident beam energy (compare to Fig. 6 at 500 and 1000 eV), but remained locked at -8±1 V. This demonstrated the hysteresis of the sample, where residual charge from the high-energy incident beam remained trapped, keeping the sample potential at a negative value regardless of subsequent lower-energy electron irradiation between the crossover energies—where positive surface charging should have occurred.

Before proceeding with pulsed-yield measurements, the sample was allowed to discharge. Based on calculations using the standard resistivity and dielectric constant for alumina (see Table 1), and treating the sample as a discharging capacitor, a 8 V surface potential should relax within a time frame ranging from minutes to hours. However, the sample was allowed to sit for one week after irradiating with light from both tungsten and mercury lamps for several hours to stimulate photo-induced conductivity (Zavyalov, 2003). Additionally, the surface was flooded occasionally with the low-energy flood gun at a current density of 50-500 nA/cm^2 for five minutes to neutralize any positive surface charge (Zavyalov, 2003).

The first pulsed yields were taken to explore the rate of sample charging from a pulsed-electron beam. Three consecutive pulsed-total yield curves (5 μs, 40-60 nA impulses) were taken without implementation of any neutralization techniques, as shown in Fig. 8. After just a few incident pulses, the yield curves were significantly dampened towards unity, even though the incident source was only depositing ~10^6 electrons/pulse over a beam-spot area of ~1 mm^2. Treating the sample as a standard parallel plate capacitor (with an area of the beam spot), this amount of charge was estimated to change the surface potential by only 10-100 mV/pulse (positive). However, a significant portion of SE's are emitted with energies less than 5 eV (see, for example, Fig. 1 for gold) such that a cumulative positive surface potential of just 1 V can significantly suppress escaping SE's. Therefore, a small change in the positive surface potential could have large effects on electron yields. These results substantiate the use of neutralization techniques (in addition to pulsed electron beam) in measuring insulator electron yields. After these initial pulsed measurements, the neutralization sources were turned on (as before), and the sample was once again allowed to sit for several days.

To further explore the rates of sample charging as well as the effectiveness of the various neutralization methods, pulsed yields were taken repeatedly at a constant energy of E_{beam}=500 eV (using single 5 μs, 40-60 nA impulses) without any neutralization between incident electron

pulses. After the initial sequence (20-30 pulses were used in each sequence) of yield measurements, the electron flood gun was turned on for five minutes to test its discharging effectiveness. Then, a second pulsing sequence was repeated. Next, the sample was irradiated with a mercury gas lamp for 15 minutes, and a third yield sequence was taken. Finally, the sample was irradiated with the tungsten filament lamp for 15 minutes, and a fourth pulsing sequence was taken. As can be seen from Fig. 9, for the initial pulsing sequence, the total electron yield decayed asymptotically towards unity (steady state condition) with repeated pulsing, consistent with the flattening of yield data in Fig. 8. In the second yield sequence (after flooding) the total yield was restored to its original uncharged value (within the error), and then once again declined at roughly the same charging rate towards unity. In the third and fourth sequence, it was observed that the mercury lamp was only partially effective in neutralizing the sample, while the tungsten lamp had no effect on the yield values. Although these results were preliminary, they showed that in the energy regime between the crossover energies, the flood gun was very effective in neutralizing positive surface potentials, providing a way to measure repeatable electron yields. However, UV and visible light irradiation in this energy regime were not as effective, but still provide methods for negative-charge neutralization for beam energies beyond the second crossover energy (Levy, 1985).

After exploring the effectiveness of the different neutralization techniques, the sample was once again allowed to discharge for a week, and then a total-yield curve for anodized aluminum was measured and fitted with various electron-yield models (Dennison, 2002) as shown in Fig. 10. Flood gun neutralization was alternated with electron beam pulsing to ensure neutralization. Additionally, yields were taken in order of increasing beam energy since it had already been observed that high-energy incident electrons could deposit negative charge that would remain trapped in the sample and influence yield measurements. From the best fit to the data, yield parameters were extracted and are given in Table 3. However, it must be mentioned that this yield data was obtained after extensive electron radiation and will need to be measured again (along with BSE and SE yield discrimination) in the near future on a virgin sample.

Silicone-RTV Samples: Methods for finding the Second Crossover Energy

Two sets of thin-film RTV coated samples were tested: the first was a DC 93-500 coating used to bond cover glass materials to solar cells on the ISS, and the second was a NuSil CV-1147 coating used to bond solar cells to Kapton™ sheeting on the ISS. Both RTV materials were relatively volatile; concerns that these materials would produce contamination layers on ISS surfaces have prompted the investigation of these thin-film materials on a conducting substrate (Dennison, 2003c). Similar contamination layers have been shown to potentially have a large impact on the charging of spacecraft surfaces (Dennison, 2001). Table 1 shows the thicknesses and electrical properties of the RTV coatings. Thicknesses were determined using a "depth of field" method with a microscope at 100 x magnification (Dennison, 2003c). The relative dielectric constants and bulk resistivities were measured using a standard impedance analyzer by the manufacturer (see Table 1). E*x situ* measurements of the volume resistivities of the thin-film silicone samples were also measured at USU using the ASTM—or capacitor resistance method—and ranged between $2\text{-}5 \cdot 10^{15}$ Ω·cm (Dennison, 2003a; Swaminathan, 2003). These insulator samples were studied primarily to determine accurate methods for measuring the total yield second crossover energy, E_2. Total yield curves as a function of incident electron energy

were also measured. A short description of each method for measuring E_2 is outlined below. Details of the measured data follow.

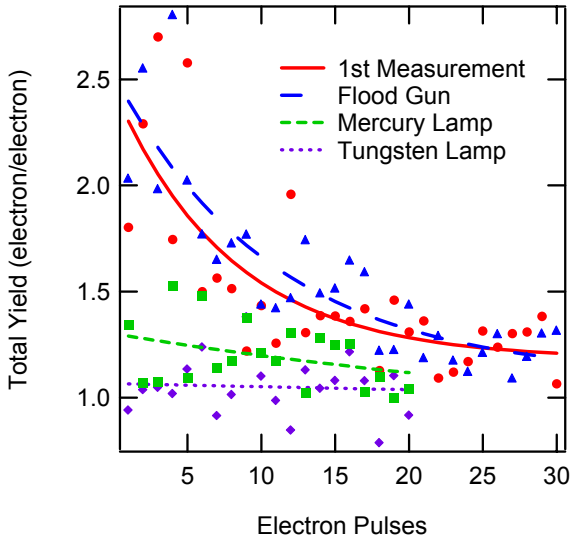

Figure 9. Dampening of total yields at 500 eV as a function of electron pulses (5 µs pulses with amplitude 50 nA) for Al2219, along with exponential fits. First yield sequence (●) and sequence following electron flooding (▲) produced similar yield decay curves indicating that flooding discharged the sample effectively. Yield sequences following mercury (■) and tungsten filament (♦) lamp irradiation remained close to unity, indicating ineffective neutralization.

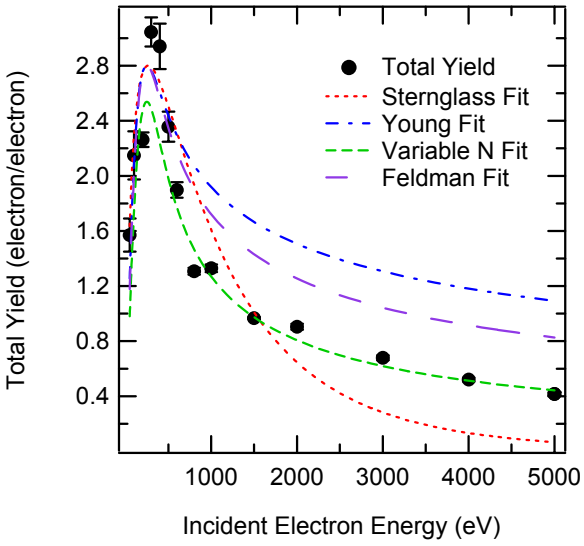

Figure 10. In contrast to Fig. 8, reliable absolute total yields were obtained with flooding the sample between yield measurements. This yield curve for Al2219 (5 µs pulses with amplitudes 50 nA, each data point was the average of 10 pulses) is fitted with various analysis models. Best estimates for yield parameters are provided in Table 3.

Pulsed Total Yield Approach: The first method was the most straightforward: total yields as a function of incident energy were taken using the pulsed-beam method, and E_2 was determined from the best fitting model to the data. The low-energy electron flood gun was used between pulses to neutralize any latent positive surface charge induced by the incident electron source.

DC-Spectra Approach: A continuous incident electron source <50 nA was used to measure DC-electron energy spectra. Regardless of the incident energy, under a DC-electron beam an insulator quickly charges to steady state where no net current arrives at or leaves the sample. When this steady state condition is met, the total yield equals unity (Reimer, 1985), and depending on the incident energy, the corresponding value of the sample potential can either be positive (for energies below E_2) or negative (for energies above E_2). As described above, the DC-SE emission spectra can be used to measure the surface potential at steady state. As the beam energy was increased towards E_2, the evolution of the surface potential was monitored using the position of the sample SE peak. The beam energy associated with the initial right-shifting of the sample SE peak (indicated by a separation of the sample SE peak from the inner grid reference peak) was taken to be the second crossover energy.

Mirroring Method: An incident electron beam at an energy beyond E_2 was used to charge the samples negatively to several hundred volts. However, as will be discussed below, it was important not to exceed the beam energy threshold corresponding to the electrical breakdown of the insulator, or else erroneous values of E_2 would result. When charged negatively with a high-energy electron beam, the sample surface potential, φ_s, of an ideal infinite-resistance insulator material will adjust such that the landing energy of incident electrons becomes equal to E_2, thus satisfying the steady state condition of $\sigma=1$. The relationship between the landing energy (E_2 at steady state), the beam energy, and the surface potential is governed by:

$$E_2 = E_{beam} - e\varphi_s \tag{1}$$

where e is electron charge and E_{beam} is the incident electron energy used to induce the negative surface potential (Reimer, 1985). However, for most thin-film insulators, some leakage current will occur either through the bulk or across the surface that must be accounted for. As a first approximation, the thin-film insulator can be treated as a planar capacitor (with the conductor substrate and charged surface acting as the electrodes) that discharges in an ohmic fashion through the bulk of the insulator. Then, the RC-time constant, τ, for discharging insulator can be written as:

$$\tau = \rho\varepsilon_r\varepsilon_0 \tag{2}$$

where ρ is the material resistivity, ε_r is the relative dielectric constant, and ε_o is the permitivity of free space. The decaying surface potential can then be estimated as a function of time as:

$$\varphi_s(t) = \varphi_{s0} \cdot e^{-t/\tau} \tag{3}$$

where φ_{so} is the initial sample potential induced by electron beam irradiation, and φ_s is the decayed potential after a time interval, t. Using Eqs. (1) through (3), one needs only to determine the original sample potential (φ_{so}) induced by E_{beam} to calculate the second crossover

energy. Note that this potential decay can be measured directly using a non-contacting surface charge probe; this forms the basis for the charge storage decay method for determining thin-film insulator resistivities developed by Frederickson (Dennison, 2003a; Swaminathan, 2003, Frederickson, 2003). However, the vacuum chamber used in these studies was not equipped with a non-contacting potential probe, so indirect methods for determining φ_s were employed.

Following an experimental procedure similar to that of Wong (1997), the samples were irradiated with a defocused electron beam to uniformly charge the samples to φ_{so}. Then, a low-amplitude, modulated probe electron beam, with a much smaller diameter was used to probe the surface potential of the insulators. In doing this, it was assumed that by using a low-amplitude modulated probe beam, the surface potential would not be significantly altered. Then, by slowly increasing the probing beam energy, E_{probe}, the kinetic energy of the incident electrons eventually overcame the potential barrier of the sample. This critical beam energy was marked by a sudden rise in the sample displacement current, and the surface potential was assumed to be equal to $\varphi_s = E_{probe}/e$. Once the surface potential was determined, E_2 was calculated from Eq. (1) after correcting for any suspected leakage current [using Eqs. (2) and (3)] that had transpired during the time of the probing experiment.

Finally, for all three methods described above, the order of measurements was planned carefully to minimize charging errors. For example, negative charge build-up (to up to several hundreds or thousands of volts) induced by beam energies beyond E_2, can be very difficult to dissipate. Consequently, precautions were taken to minimize sample exposure to the high-energy (>1 keV) incident electrons until all lower-energy (<1 keV) measurements were made by initially taking pulsed-yield measurements (in order of increasing incident energies), followed by DC-spectra at energies near E_2, and lastly, the mirror method technique (that induced significant negative charging).

Pulsed-yields as a function of incident energy were taken on samples 1 and 6 using 5 μs, 50 nA incident pulses. The sample surface was neutralized with the flood gun after each incident electron pulse, and ten pulsed measurements were averaged for each data point,. The pulsed-yield measurements were started at beam energies of 100 eV, and then increased to 1 keV (yields beyond 1 keV were not taken until after DC-spectral measurements). The yield curves along with their best-fitting semi-empirical models are shown in Figs. 11 and 12. When the total yield curves began to approach unity for samples 1 and 6 (close to E_2), the electron gun was switched from pulsed to continuous-emission mode, and DC-spectra were taken (at ~30 nA incident beam current) on the samples as the beam energy was increased. Eventually, E_2 was crossed, and double-peak SE emission spectra (as described above) were observed due to negative charging as shown in Figs. 13 and 14. Estimates for E_2 as determined from both the pulsed-yield (best fitting model estimate) and DC-spectral methods are given in Table 1. Of the two techniques, the spectral measurements were considered to be a more precise method for determining E_2 since SE emission energies were very sensitive to sample potentials of even a few volts (causing the double-peaks in Figs. 13 and 14). However, there were concerns that for the DC-spectral method, continuous electron-beam bombardment could have altered yield parameters, including E_2, resulting from charge deposition in the bulk of the material.

When pulsed-yield and DC-spectral measurements were completed, mirror-method potential measurements were taken on all samples for E_{beam}=2 keV, 2.3 keV, 2.5 keV, and 3 keV (measurements were always taken in order of increasing beam energy on a given sample). The RTV samples were irradiated with a defocused (~10 mm diameter for uniform charging) electron beam at 100 nA for 5 minutes for each beam energy. During this irradiation period, DC sample current was monitored to check for dielectric breakdown of the insulators. At these incident energies, sample current was found to be lower than the noise level ±1 nA, except for sample 6 (see below). After this irradiating period, the electron gun was suppressed temporarily, and the beam energy was decreased of the insulator film as outlined above. Shown in Fig. 15 is a plot of the sudden rise in sample displacement current in response to the incident probe beam energy where the critical energy was reached, and the sample potential barrier was breached.

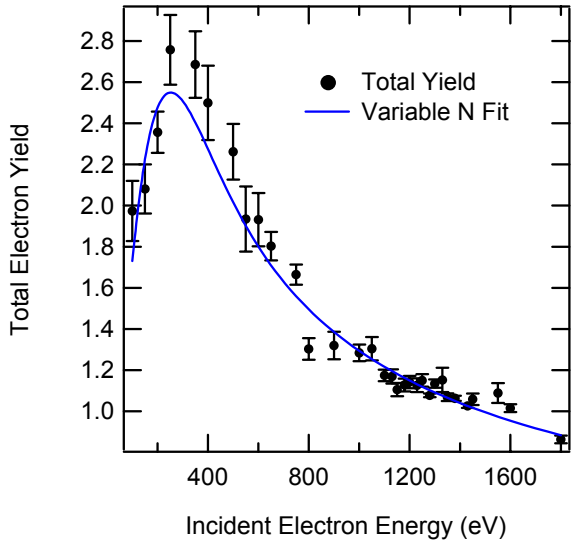

Figure 11. Pulsed-yield curve versus beam energy for CV-1147 sample 1 with flood gun neutralization after each pulse. Each yield point was the average of 10 pulsed-yield measurements (5 μs pulse with amplitude 50 nA) with standard errors as the error bars. The best model estimates for the total yield parameters were: σ_{max}=2.5±0.1 at E_{max}=250±10 eV, E_1=40±20 eV, and E_2=1470±40 eV. Model estimates for the maximum yield were low compared to the data.

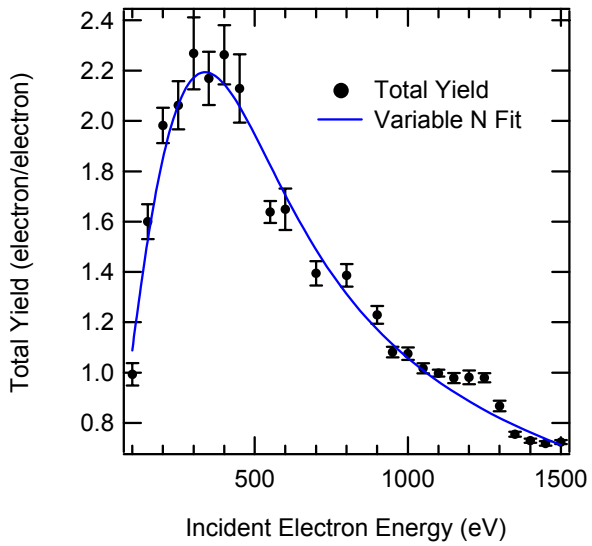

Figure 12. Pulsed-yield curve versus beam energy for DC 93-500 sample 6 with flood gun neutralization after each pulse. Each yield point was the average of 50 pulsed-yield measurements (5 µs pulse with amplitude 50 nA) with standard errors as the error bars. The best model estimates for the total yield parameters were: σ_{max}=2.2±0.1 at E_{max}=340±10 eV, E_1=90±10 eV, and E_2=1050±30 eV. Model estimates for the maximum yield were low compared to the data.

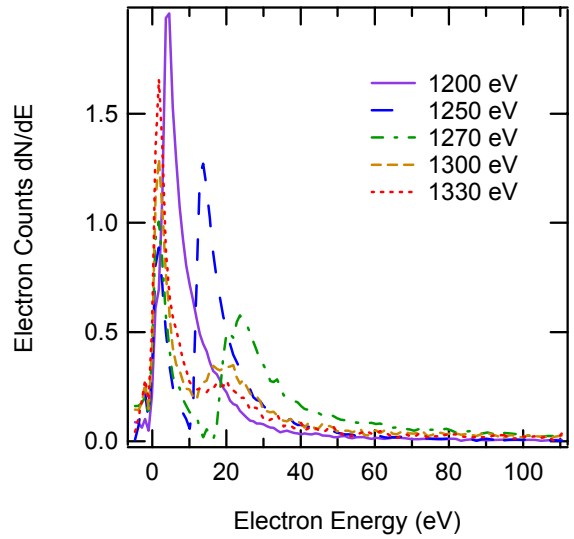

Figure 13. Shown are evolving SE spectra for sample 1 for increasing electron beam energies of 1200 eV (solid), 1250 eV (long dash), 1270 eV (dash-dot), 1300 eV (short dash), and 1330 eV (dot). The emergence and right-shifting trend of the 2nd SE peak was caused by a negative sample potential caused by the incident electron beam energy exceeding E_2. These spectra indicated a crossing of E_2 at 1200-1250 eV.

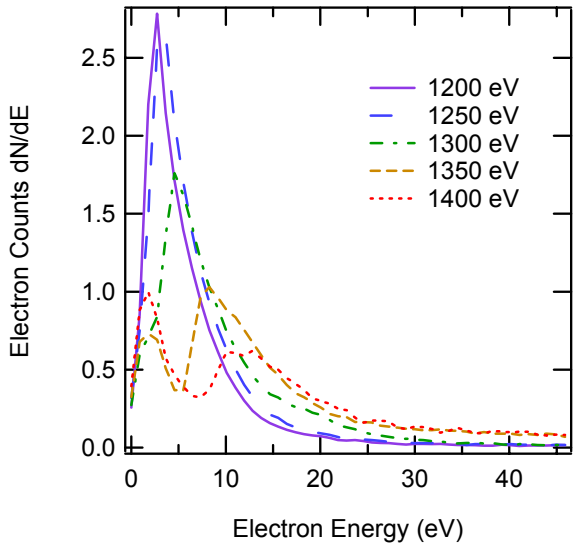

Figure 14. Shown are evolving SE spectra for sample 6 for increasing incident electron beam energies of 1200 eV (solid), 1250 eV (long dash), 1300 eV (dash-dot), 1350 eV (short dash), and 1400 eV (dot). These spectra indicated a crossing of E_2 at 1250-1300 eV.

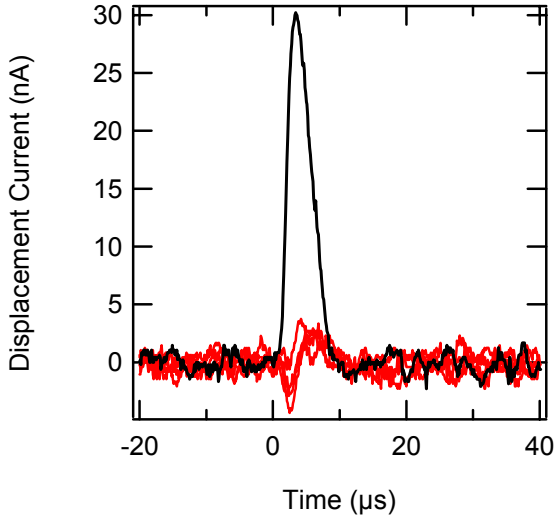

Figure 15. Shown is a plot of the rise in displacement current of a probing electron pulse (5 μs at 100 nA) once the incident energy overcame the surface potential barrier induced by a high-energy electron beam. In this case, the small displacement currents are induced by probe beam energies ranging from 900-1200 eV, while the large displacement current curve occured at 1250 eV. From this, the surface potential was taken to be 1250 eV.

Table 2. Mirror method results for the sample surface potential and E_2, for RTV samples at different irradiation energies, E_{beam} calculated from Eqs. (1) and (3) using the measured surface potential, φ_s and a RC time constant of 4 min. as determined from Eq. (2). Variations in E_2 resulted from uncertainties in the measurement time interval of 1-3 min. E_{beam} values indicated with a * induced surface potentials,φ_s, exceeding the sample dielectric breakdown potential (shown in Table 1), and therefore produced inaccurate estimates for E_2 (also indicated by *). Sample 6 appeared to have already undergone electrical breakdown at E_{beam} <2 keV.

Sample	E_{beam} (eV)	φ_s (V)	E_2 (eV)
RTV 1	2000	475 ± 25	1200±200
	2500*	775 ± 25	1150±300*
	3000*	875 ± 25	1500±400*
RTV 2	2000	500 ± 100	1100±200
	2300*	850 ± 100	800±400*
	2500*	1250 ± 50	300±550*
	3000*	1800 ± 100	-100±800*
RTV 5	2000	290 ± 10	1500±100
	2300	525 ± 25	1400±200
	2500	625 ± 50	1400±300
	3000*	1140 ± 10	1000±500*
RTV 6	2000*	175 ± 25	1700±100*
	2500*	150 ± 50	2200±100*
	3000*	250 ± 50	2500±100*

Table 3. Summary of measured total electron yield parameters and the electrical breakdown potentials of studied materials. Maximum yields, maximum yield energies were taken directly from the raw data since estimates from the fitting models were too low. Crossover energies were obtained from the best-fit of the yield data, except for CV-1147 and DC93-500, where estimates for E_2 were obtained from the SE spectral method. Measured breakdown potentials were obtained from SE spectra for anodized Al and the mirror potential method for the two RTV samples.

Sample	Maximum Total Yield	Maximum Total Yield Energy (eV)	First Crossover Energy (eV)	Second Crossover Energy (eV)	Measured Breakdown Potential (V)
Gold	1.8±0.1	600±50	100±20	10000±1000	Not applicable
Al2219	3.0±0.1	300±50	50±10	1400±100	>21
CV-1147	2.8±0.2	250±50	40±20	1225±25	700±200
DC93-500	2.3±0.2	350±50	90±10	1275±25	850±250

Mirror-method results for measured surface potentials along with calculated values for E_2 were calculated using Eqs. (1) through (3). Using the manufacturer material specification data provided in Table 1, estimates for the leakage RC time constant, τ, were calculated to be 4 min. [from Eq. (2)] for all RTV samples. In comparison, probing measurements lasted anywhere from 1 to 3 min. Consequently, during the course of an experiment, the sample surface potentials decreased as determined by Eq. (3). After making these corrections, estimates for E_2 were calculated using Eq. (1), and are given in Table 2 for different values of E_{beam}.

From the data in Table 2, it can be seen that E_2 values derived at higher E_{beam} (>2.5 keV) were typically inconsistent with respect to values derived from E_{beam}=2.0 keV, and were also prone to large errors. It is conceivable that electrical breakdown (in the form of small sustained arcs through the bulk of the films) occurred at higher-energy electron irradiation as indicated by * in Table 2. Dielectric breakdown potentials of the four samples were calculated based on dielectric strength values (see Table 1). As seen in Table 2, (with the exception of sample 6, see below), E_2 values were consistent for each sample for surface potentials, φ_s, lower than the calculated breakdown potentials. This observation provides some evidence that the mirroring method approach to finding E_2 was obfuscated by low breakdown potentials of thin-insulating films, and may be a more suitable method for finding the crossover energies of thicker samples. Table 1 summarizes all estimates for E_2 as determined from the three methods described above.

Finally, in contrast to the other RTV samples, the surface potential of sample 6 did not rise with increasing radiation energy, and stayed at relatively low potentials between 150 V to 300 V as shown in Table 2. As mentioned earlier, for sample 6, a sample current of ~2 nA was measured at beam energies ranging from 2-3 keV. It was speculated that the sample had undergone dielectric breakdown (prematurely) at beam energies <2 keV. This assumption was consistent with the fact that sample 6 had been prepared with the thinnest RTV coating (compared to the other three samples), and should therefore have demonstrated the lowest breakdown potential (see Table 1). Other samples displayed similar breakdown behavior at higher beam energies. For example, when E_{beam} was pushed to 5000 eV at 30 nA for sample 1 the sample current suddenly rose >20 nA. Then, upon decreasing E_{beam} to energies as low as 800 eV (keeping the incident current at ~30 nA), the sample remained open to current conduction on the order of 4 nA. Although the electrical breakdown of sample 6 did not influence pulsed-yield or DC-spectral estimates for E_2, since these measurements were taken before mirror method measurements, E_2 values derived from the mirror method were considered to be inconclusive for this sample.

Summary and Conclusions

Total electron yield measurements have been presented for one conductor and three types of insulators used in ISS construction. SE emission spectra demonstrated shifting energy distributions in response to samples with nonzero surface potentials. The spectra on gold demonstrated that as the sample surface potential was biased negatively, the SE peak shifted to higher energies (to the right in the spectral graphs) by an amount that corresponded to the applied sample potential. This technique was used to determine the potentials of charged insulator samples under continuous electron beam bombardment.

Measurements on Al2219 chromic-acid anodized aluminum showed that charging can occur very quickly on an insulator sample, even at low electron fluences of ~10^6 electrons/pulse over a ~1 mm^2 area. Charging, both under continuous and pulsed-electron irradiation, drove the total yield of the sample towards unity as current steady state was reached. Additionally, it was found that at a critical incident electron energy (initially 1500 eV, then 1250 eV on a subsequent run), the surface potential became sufficiently high (>20 V) to initiate dielectric breakdown of the thin anodized layer. After irradiating the sample with high incident energies of 5 keV, it was found that trapped charge in the sample maintained the surface potential at a negative value on the order of ten volts, even while being irradiated with an electron beam at energies (500 eV and 1000 eV) that should have induced positive surface charging. This behavior may later provide information on trapped internal charge distributions caused by higher-energy (> 1 keV) electron irradiation. Finally, electron yields were measured for the sample, and results are reported in Table 3.

With the two types of RTV-Silicone adhesive samples (CV-1147 and DC93-500), three approaches were explored for determining the second crossover energy, E_2: i) the pulsed-total yield approach; ii) the DC-spectral approach; iii) and the mirroring method approach. Of these three methods, the DC-spectra approach was assumed to be most sensitive to sample negative charging, and therefore a more accurate method for determining E_2. However, there were concerns that continuous electron beam irradiation may have altered yield parameters, including E_2. Also, it became apparent that the mirror method for determining E_2 was only valid when the beam energy threshold for dielectric breakdown was not exceeded. This may restrict the mirror method to thicker insulators (>100 μm). Results for the three methods are reported in Table 1. Best estimates for yield parameters for all the materials studied are reported in Table 3.

From these measurements, continuous- and pulsed-beam techniques for determining insulator yield parameters have been demonstrated. For both Al2219 and RTV samples, there was also clear evidence that >1 keV electron bombardment left residual charge under the surface that affected subsequent yields. Clearly, more work is needed to quantitatively asses charging effects on insulator potentials and electron emissions for different materials. Available tools and techniques demonstrated here are adequate to perform further required tests with carefully controlled sample bombardment history.

Acknowledgments

The work presented was supported in part by the NASA Space Environments and Effects (SEE) Program, the Boeing Corporation, and a NASA Graduate Fellowship. Samples were supplied by Boeing, the Materials, Processes, and Manufacturing Department at NASA Marshall Space Flight Center, and Sheldahl, Inc.

References

1. John Alred, Boeing Corporation (private communications), 2001.

2. G. Auday, Ph. Guillot, and J. Galy, "Secondary emission of dielectrics used in plasma display panels," J. Appl. Phys. 88 (8), 4871-4874 (2000).

3. M. Belhaj, S. Odof, K. Msellak, and O. Jbara, "Time-dependent measurement of the trapped charge in electron irradiated insulators: Applications to Al_2O_3-sapphire," J. Appl. Phys. 88 (5), 2289-2294 (2000).

4. M.R. Carruth Jr., T. Schneider, M. McCollum, M. Finckenor, R. Suggs, D. Ferguson, I. Katz, R. Mikatarian, J. Alred, and C. Pankop, "ISS and space environment interactions without operating plasma contactor," AIAA Paper #2001-0401, Proceedings for the 39th Aerospace Sciences Meeting and Exhibit, Reno, Nevada, Jan. 9-11, 2001.

5. J. Cazaux, "Some considerations on the secondary electron emission δ, from e^- irradiated insulators," J. Appl. Phys. 85 (2), 1137-1147 (1999).

6. CRC Handbook of Chemistry and Physics, 82nd Ed. (CRC Press, Boca Raton, FL, 2001).

7. Robert Davies, "Measurement of Angle-resolved Secondary Electron Spectra," PhD Dissertation, Utah State University, Logan, Utah, May 1999.

8. R.E Davies and J.R. Dennison, "Evolution of Secondary Electron Emission Characteristics of Spacecraft Surfaces," J. Spacecraft and Rockets, 34, 571-574 (1997).

9. J.R. Dennison, A. R. Frederickson, Prasanna Swaminathan, "Charge Storage, Conductivity And Charge Profiles Of Insulators As Related To Spacecraft Charging," Proceedings of the 8th Spacecraft Charging Technology Conference, October 20-24, 2003a, Huntsville, Alabama.

10. J.R. Dennison, C.D. Thomson, J. Kite, V. Zavyalov, Jodie Corbridge, "Materials characterization at Utah State University: facilities and knowledgebase of electronic properties of materials applicable to spacecraft charging," Proceedings of the 8th Spacecraft Charging Technology Conference, October 20-24, 2003b, Huntsville, Alabama.

11. J.R. Dennison, C.D. Thomson, and Jodie Corbridge, "Electronic Properties of ISS Materials," Boeing Company Final Report, Contract No. M/C H014-B419, 2003c.

12. J.R. Dennison, J. Kite, C.D. Thomson, Jodie Corbridge, Robert Berry, and Carl Ellsworth, "Final Report Part IV: Additional Materials Reports," NASA Space Environments and Effects Program Grant, Electronic Properties of Materials with Application to Spacecraft Charging, May 2003d.

13. J.R. Dennison, W.Y. Chang, N. Nickles, J. Kite, C.D. Thomson, Jodie Corbridge, and Carl Ellsworth, "Final Report Part III: Materials Reports," NASA Space Environments and Effects Program Grant, Electronic Properties of Materials with Application to Spacecraft Charging, September 2002.

14. J.R Dennison, Jason Kite, W.Y. Chang, and R.E. Davies, "Absolute and Differential Spacecraft Charging as a Result of Evolving Surface Contamination," Proceedings of the 7th Spacecraft Charging Technology Conference, (2001, Noordwijk, Netherlands).

15. Dow Corning 93-500 Space-Grade Encapsulant Product Information, Ref. No. 10-1062A-01, DC 3367, (Dow Corning Corporation, Midland MI, 05/01/1998).

16. A.R. Frederickson and J. R. Dennison, "Measurement of Conductivity and Charge Storage in Insulators Related to Spacecraft Charging," accepted for publication in IEEE Trans. Nuc. Sci., December, 2003.

17. K. Goto and K. Ishikawa, "Secondary electron emission from diffusion pump oils II. δ-η analysis for DC-705," J. Jap. Appl. Phys. 7 (3), 227-231 (1968).

18. P. Girard, P. Charpenel, and H. Martin, "Determination of the noncharging electron-beam energy on insulators," J. Appl. Phys. 71 (6), 2871-2876 (1992).

19. Goodfellow online catalogue, 2003.

20. K. Ishikawa and K. Goto, "Secondary electron emission from diffusion pump oils I," J. Jap. Appl. Phys. 6 (11), 1329-1335 (1967).

21. O. Jbara, M. Belhaj, S. Odof, K. Msellak, E.I. Rau, and M.V. Andrianov, "Surface potential measurements of electron-irradiated insulators using backscattered and secondary electron spectra from an electrostatic toroidal spectrometer adapted for the scanning electron microscope applications," Rev. Sci. Instrum. 72 (3), 1788-1795 (2001).

22. J.B. Johnson, "Secondary electron emission from targets of Barium-Strontium Oxide," Phys. Rev. 73 (9), 1058 (1948).

23. J.B. Johnson and K.G. McKay, "Secondary electron emission of crystalline MgO," Phys. Rev. 91 (3), 582-587 (1953).

24. I.Krainsky, W. Lundin, W.L. Gordon, R.W. Hoffman, Secondary Electron Emission Yield Annual Report for Period July 1, 1980 to June 30, 1981, Case Western Reserve University, Cleveland, OH, 1981 (unpublished).

25. L. Levy, D. Sarrail, and J.M. Siguier, "Conductivity and secondary electron emission properties of dielectrics as required by NASCAP," Proceedings of the Third European Symposium on Spacecraft Materials in Space Environment, Noordwijk, The Netherlands, October 1-4, 1985.

26. A.Melchinger, and S. Hofmann, "Dynamic double layer model: Description of time dependent charging phenomena in insulators under electron beam irradiation," J. Appl. Phys. 78 (10), 6224-6232 (2003).

27. Y. Mizuhara, J. Kato, T. Nagatomi, Y. Takai, and M. Inoue, "Quantitative measurement of surface potential and amount of charging on insulator surface under electron beam irradiation," J. Appl. Phys. 92 (10), 6128-6133 (2002).

28. C.W. Mueller, "The secondary electron emission of pyrex glass," J. Appl. Phys. 16, 453-458 (1945).

29. NASA Marshall Space Flight Center Materials, Processes, and Manufacturing Department, 2002-2003.

30. NuSil CV-1147 Controlled Volatility RTV Silicone Atomic Oxygen Protective Coating Product Profile, NT/061801/REVA (NuSil Technology, Carpinteria, CA, 06/18/2001).

31. NuSil CV-1147 Material Safety Data Sheet, (NuSil Technology, Carpinteria, CA, 03/09/1998).

32. L. Reimer, Scanning Electron Microscopy. Physics of Image Formation and Microanalysis, (Springer-Verlag., 1985), pp. 119-121.

33. Todd Schneider, NASA Marshall Space Flight Center Materials, Processes, and Manufacturing Department, (private communications) 2002-2003.

34. H. Seiler, "Secondary electron emission in the scanning electron microscope," J. Appl. Phys. 54 (11), R1-R18 (1983).

35. A.Shih, J. Yater, P. Pehrsson, J. Butler, C. Hor, and R. Abrams, "Secondary electron emission from diamond surfaces," J. Appl. Phys. 82 (4), 1860-1867 (1997).

36. Prasanna Swaminathan, A. R. Frederickson, J.R. Dennison, Alec Sim, Jerilyn Brunson, and Eric Crapo, "Comparison Of Classical And Charge Storage Methods For Determining Conductivity Of Thin Film Insulators," Proceedings of the 8th Spacecraft Charging Technology Conference, October 20-24, 2003, Huntsville, Alabama.

37. Charles Swenson, "Calibrating the Floating Potential Measurement Unit," Proceedings of the 8th Spacecraft Charging Technology Conference, October 20-24, 2003, Huntsville, Alabama.

38. J.P. Vigouroux, J.P. Duraud, A. Le Moel, C. Le Gressus, and D.L. Griscom, "Electron trapping in amorphous SiO_2 studied by charge buildup under electron bombardment," J. Appl. Phys. 57 (12), 5139-5144 (1985).

39. N. Rey Whetten, "Cleavage in high vacuums of alkali halide single crystals-secondary electron emission," J. Appl. Phys. 35 (11), 3279-3282 (1964).

40. N. Rey Whetten and A.B. Laponsky, "Secondary Electron Emission from MgO Thin Films," J. Appl. Phys. 30 (3), 432-435 (1959).

41. N. Rey Whetten and A.B. Laponsky, "Secondary electron emission of single crystals of MgO," J. Appl. Phys. 28, 515 (1957).

42. W.K. Wong, J.C.H. Phang, and J.T.L. Thong, "Estimation of the second crossover in insulators using the electrostatic mirror in the scanning electron microscope," Appl. Phys. Lett. 71 (9), 1270-1272 (1997).

43. W. Yi, S. Yu, W. Lee, I.T. Han, T. Jeong, Y. Woo, J. Lee, S. Jin, W. Choi, J. Heo, D. Jeon, J.M. Kim, "Secondary electron emission yields of MgO deposited on carbon nanotubes," J. Appl. Phys. 89 (7), 4091-4095 (2001).

44. Y.C. Yong, J.T.L. Thong, and J.C.H. Phang, "Determination of secondary electron yield from insulators due to a low-kV electron beam," J. Appl. Phys. 84 (8), 4543-4548 (1998).

45. S. Yu, T. Jeong, W. Yi, J. Lee, S. Jin, J. Heo, and D. Jeon, "Double-to single-hump shape change of secondary electron emission curve for thermal SiO_2 layers," J. Appl. Phys. 79 (20), 3281-3283 (2001).

46. V. Zavyalov, C.D. Thomson, J.R. Dennison, "Instrumentation for studies of electron emission and charging from insulators," Proceedings of the 8th Spacecraft Charging Technology Conference, October 20-24, 2003, Huntsville, Alabama.